RSC Advances

PAPER

View Article Online
View Journal | View Issue

Cite this: *RSC Adv.*, 2017, **7**, 27224

Synthesis and characterization of sulfophenyl-functionalized reduced graphene oxide sheets†

Benjamin Diby Ossonon and Daniel Bélanger *

Received 16th December 2016
Accepted 10th May 2017

DOI: 10.1039/c6ra28311j

rsc.li/rsc-advances

We report the modification of graphene oxide (GO) by thermal reduction to obtain reduced graphene oxide (RGO) and subsequent modification by sulfophenyl groups as well as the characterization of these materials by thermogravimetric analysis coupled with mass spectroscopy (TGA-MS). The chemical modification of RGO was carried out by the spontaneous reaction of RGO with *in situ* generated sulfophenyl diazonium ions. The three different types of materials were also characterized by elemental analysis, Fourier transform infrared spectroscopy (FTIR), Raman spectroscopy and X-ray photoelectron spectroscopy (XPS). The characteristic absorption band at 1034 and 1160 cm^{-1} in the FTIR spectrum of the sulfophenyl-modified RGO (SRGO), as well as Raman spectroscopy and TGA-MS data indicated that sulfophenyl groups were successfully grafted on RGO. The presence of organic molecules at the SRGO surface was also demonstrated by elemental analysis, transmission electron microscopy, energy dispersive X-ray spectroscopy and XPS. TGA data and elemental analysis results showed that the loading of sulfophenyl groups was about 12 wt% and UV-visible-near IR spectroscopy confirms the slight increase of the optical band gap of RGO after covalent grafting of sulfophenyl groups on its surface.

1 Introduction

Graphene is a two-dimensional carbon material consisting of a single-atom-thick graphitic layer that has been used in electronic devices,[1,2] composite materials[3,4] and energy storage systems.[5–9] Graphene is commonly produced from natural graphite, which is widely available at low cost.[10] However, graphene is not directly prepared from graphite. Instead it is obtained by the reduction of graphene oxide (GO), previously produced by the Hummers method.[11] The reduction of GO to graphene restores the electronic properties of graphene and has been performed by using reducing agents such as hydrazine (N_2H_4),[12,13] sodium borohydride ($NaBH_4$),[14,15] dimethyl hydrazine[3] and hydriodic acid (HI).[16,17] However, these reducing agents may be harmful to the environment or too expensive when used for mass production of graphene. Also, the quality of the reduced GO, RGO, strongly depends on the reducing agent and other experimental conditions.[18] Alternatively, thermal reduction, which is considered a green method because no hazardous chemicals are required, can also afford RGO.

Graphene possesses a zero band gap that severely limits its applications due to its chemical inertness.[4,19] Opening the band gap of graphene and its derivative by doping, intercalation or grafting by organic molecules would be useful for applications mentioned above.[6,8] Importantly, functionalization with organic molecules led to a good dispersion of graphene in common organic solvents.[20] For several large-scale applications, RGO is a more widely used and attractive material than graphene. Similarly, its functionalization is important to modify its properties and open up its applications to the areas.

Here we report, a detailed investigation of graphene oxide (GO), reduced graphene oxide (RGO) and sulfophenyl-modified RGO (SRGO) by thermogravimetric analysis coupled with mass spectrometry (TGA-MS) analysis. The TGA-MS data confirmed the covalent grafting of sulfophenyl groups on RGO. The three materials were also characterized by nitrogen gas adsorption, FTIR, four-point probe measurements as well as by Raman and X-ray photoelectron spectroscopy.

2 Experimental

Preparation of graphene oxide (GO)

Graphene oxide was synthesized from natural graphite (<44 μm, 99.99%, supplied by Sigma-Aldrich) through the Hummers method[11] which has been improved to be more environmentally friendly and produce graphene in good yield (95%). The graphite is first pre-oxidized by mixing graphite powder (5 g) with concentrated sulfuric acid (H_2SO_4, 12.5 mL), potassium persulfate ($K_2S_2O_8$, 2.5 g) and phosphorus pentoxide (P_2O_5, 2.5 g). The mixture was heated at 80 °C for 6 hours. After dilution with 500 mL of H_2O, the mixture was stirred at room temperature overnight. After that, the product is recovered by centrifugation and washed thoroughly with Nanopure water until the

Département de chimie, Université du Québec à Montréal, Case Postale 8888, Succursale Centre-Ville, Montréal, QC, H3C 3P8, Canada. E-mail: belanger.daniel@uqam.ca

† Electronic supplementary information (ESI) available. See DOI: 10.1039/c6ra28311j

filtrate has a pH close to 7 (neutral). The product obtained is then dried at room temperature for one day. Then, the pre-oxidized graphite is dispersed in H_2SO_4 (0 °C, 115 mL). The temperature of the mixture is carefully controlled to not exceed 10 °C. Subsequently, potassium permanganate ($KMnO_4$, 15 g) is gradually added with constant stirring for 1 hour. The dispersion is then incubated at 35 °C for 2 h and this is followed by the addition of Nanopure water (225 mL) in small portions (15 mL) to control the temperature of the mixture, which must remain below 50 °C. In order to completely dissolve the $KMnO_4$ remaining, hydrogen peroxide (H_2O_2 30%, 12.5 mL) was immediately added at the end of a second dilution (H_2O, 700 mL), and the mixture is stirred for 48 hours. Finally, the suspension is filtered, washed first with HCl (10%) to remove residual metal ions, and repeatedly with Nanopure water until the pH of filtrate becomes neutral. The filtrate is quickly tested by adding a few drops of 1 M NaOH to verify the presence of metal ions in GO. The product obtained (graphite oxide) is then dried in air. The resultant graphite oxide was dispersed in Nanopure water kept in the ultrasonic bath for 24 hours to maximize exfoliation. A homogeneous and stable colloidal suspension for several months is obtained (Fig. 1, GO).

Preparation of reduced graphene oxide (RGO)

The reduced graphene oxide (RGO) is obtained by thermal reduction of GO in Ar/5% H_2 at various temperatures for 2 h. The resulting RGO can be dispersed in water and the dispersion stayed stable for few hours, as shown in Fig. 1.

Covalent attachment of 4-sulfophenyl groups by the diazonium chemistry on RGO surface

Typically, a mass of 100 mg of RGO is dispersed in 100 mL of an acetonitrile/H_2O (50 : 50, v/v) mixture and a homogeneous and stable colloidal suspension was obtained after sonication, for 30 min. Then, 15 mmol of amine (4-aminobenzenesulfonic acid) and an excess of sodium nitrite (22.5 mmol; 1.5 equiv. compared to the amine) was directly added to the dispersion. The mixture was dispersed by sonication during an additional 30 min to completely dissolve the reagents and this was followed by the addition of 10 mL of concentrated HCl. The reaction mixture remained under agitation for 24 hours at room temperature. The dispersion was finally vacuum filtered on a Nylon filtration membrane having a pore size diameter of 0.47 μm (Pall) and the resulting powder was successively washed with a mixture acetonitrile/Nanopure water, acetonitrile, DMF, methanol and acetone. Finally, the resulting modified-RGO (SRGO) was dried under vacuum at 80 °C overnight before being subjected to thermal annealing under Ar atmosphere at 250 °C for 1 h. The resulting powder is dispersible in water and remains stable for several days (Fig. 1, SRGO).

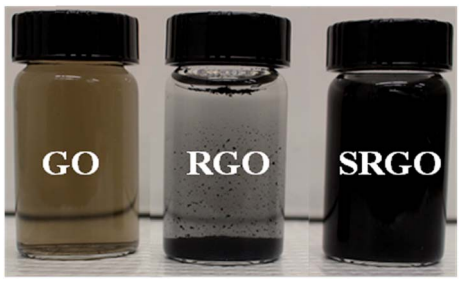

Fig. 1 Optical images of GO, RGO and SRGO dispersed in water at the concentration of 0.5 mg mL^{-1}.

Morphological, structural and optical characterization

The morphology of the graphene materials was investigated by transmission electron microscopy (TEM) using a 200 keV JOEL JEM-2100F model transmission electron microscope operated with a bright field image. The energy band gap of reduced graphene oxide (RGO) and sulfophenyl-modified reduced graphene oxide (SRGO) was determined at room temperature using UV/VIS/NIR Spectrophotometer Lambda 750. For these analyses, the graphene samples were dispersed in NMP (*N*-methyl-2-pyrrolidone) to form colloidal suspensions (0.03 mg mL^{-1}). The optical band gap (E_g) of RGO and SRGO were estimated using the Tauc–David Mott equation (eqn (1)).[21–25]

$$(\alpha h\nu)^n = A(h\nu - E_g) \quad (1)$$

where $h\nu$ is the photon energy (h is Planck's constant, ν is the light frequency), α the absorption coefficient, E_g is the optical gap, the nature of band transition characterized by $n = 1/2$, 2, 3/2 and 3 and the constant, which is different for each transition.[25] Fourier transform infrared (FTIR) spectroscopy was employed to characterize the graphene materials using the Nicolet 6700 FTIR in the 3800–700 cm^{-1} region. XPS spectra were collected using the spectrophotometer PHI 5600-ci (Physical Electronics, Eden Prairie, MN, USA). The excitation source used for survey spectra was by standard Al K_α (1486.6 eV) X-rays at 400 W and for core level spectra, by Mg K_α (1253.6 eV) X-rays at 150 W. The analyses were performed without charge compensation at an angle of 45° with the surface. The detector aperture was set at 5 and the surface area analyzed was 0.016 cm^2. The core level spectra were curve-fitted with the Casa XPS software by using mixed Gaussian–Lorentzian product function (70% Gaussian). Each spectrum was corrected with respect to C 1s at 284.5 eV (C sp^2 graphite like carbon) and a Shirley type background subtraction was performed before curve-fitting. Thermogravimetric analysis coupled with mass spectroscopy (TGA-MS) was carried out with a thermal gravimetric analyzer (TA Instruments TGA (Q500)/Discovery MS). Samples of typically 2 mg were placed in Pt pans and heated from 30 to 900 °C with a temperature ramp of 5 °C min^{-1}, under flowing helium (He) atmosphere. Raman spectroscopy measurements were performed using a micro-Raman system (UHTS300) with excitation from an argon ion laser beam (532 nm) at low power level (2 mW) in order to avoid damaging the organic functional groups. The surface area and pore volume were quantified using the Brunauer–Emmett–Teller (BET) method from the adsorption branch data set recorded for P/P_0 values between 3×10^{-1} and 5×10^{-2}. The volume of nitrogen adsorbed was recorded for relative pressures (P/P_0) ranging from 1×10^{-6} to 1. The density functional theory (DFT) was used to provide a much more

accurate approach to pore size analysis.[26] Prior to measurements, the sample was degassed for 4 h under vacuum. Electronic conductivity of GO, RGO and SRGO films was obtained at room temperature by using a 4-point probe measurement by using a Keithley 6220 DC precision current source (US). The GO, RGO and SRGO films were obtained as follows. The samples were dispersed in water by ultrasonication for 30 min and the resulting suspensions were filtered through a polytetrafluoroethylene (PTFE) membrane filter by vacuum filtration and dried under vacuum at 70 °C overnight. The electrical conductivities were calculated by using the following equation:[27]

$$\left(\sigma,\ \mathrm{S\ cm^{-1}}\right) = \frac{1}{\rho} = \frac{\ln 2}{\pi d R} = \frac{1}{4.53 d R} \quad (2)$$

where ρ (Ω cm) is the resistivity, d (cm) is the sample thickness and R (Ω) is the resistance.

3 Results and discussion

Morphological characterization of RGO and SRGO

TEM images were employed to study the morphology of RGO and SRGO. Fig. 2a clearly shows that the RGO sheets are almost transparent, suggesting that they consist of a few layers. The EDX spectrum (Fig. 2a) of the RGO sample confirms the presence of only carbon and of a small amount of oxygen (O/C: 0.08). On the other hand, Fig. 2b exhibits aggregated and wrinkled sheets.

This observation demonstrates that the attachment of organic groups on the surface of graphene sheets favour their overlapping and folding.[20,28–30] It is an indirect way to confirm the functionalization of RGO sheets with organic molecules. Energy dispersive spectrum of SRGO (Fig. 2b) shows sulfur peaks that confirm the presence of sulfophenyl groups on reduced graphene oxide.

Optical band gap

The visible/near-infrared absorption spectra of RGO and SRGO presented in Fig. 3a and b were measured to evaluate the optical band gap of graphene materials. The absorption spectra of RGO and SRGO show an absorption band around 1430 nm. The optical band gap (E_g) of the graphene materials was estimated from the absorption spectra (ESI, Fig. S1†) by plotting $(\alpha h\nu)^2$ *versus* $h\nu$, as shown in Fig. 3c and d, and extrapolating the linear region of the curve to the x-axis.[31] The band gap slightly increased following RGO functionalization, from 0.95 (ref. 32) to 1.18 eV SRGO, indicating that the optical properties of RGO have been changed after chemical modification with sulfophenyl groups.[33]

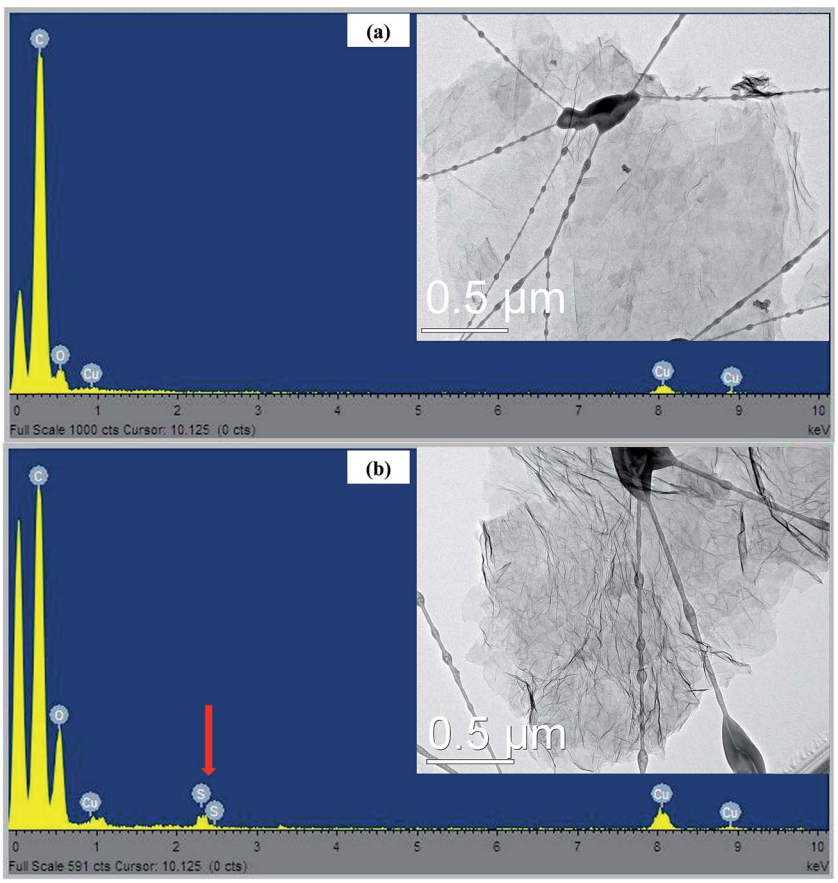

Fig. 2 EDX spectra and TEM images of (a) RGO and (b) SRGO.

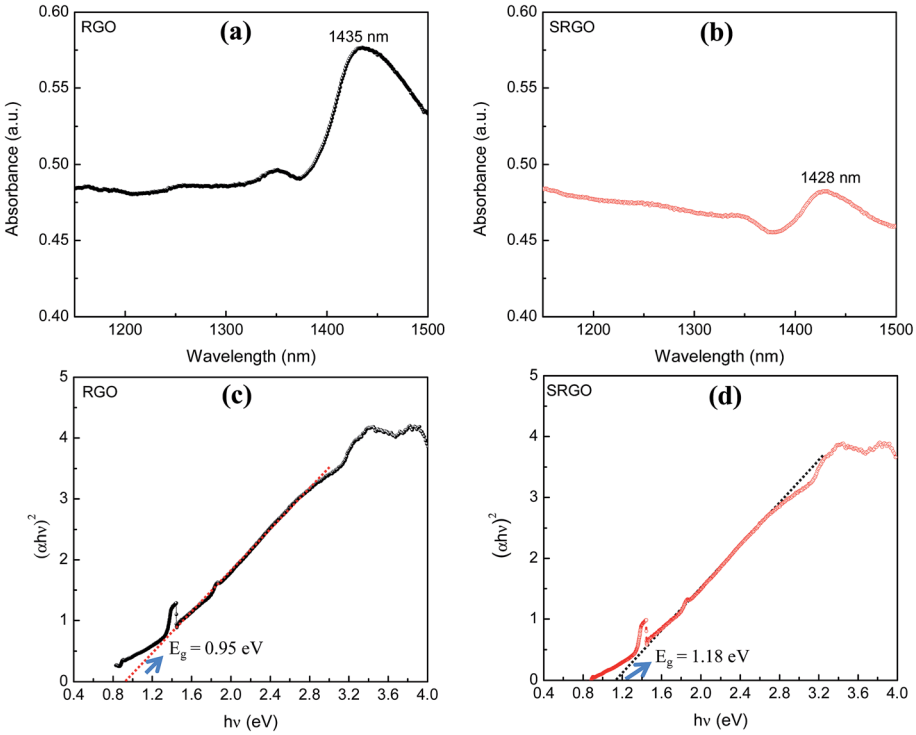

Fig. 3 Visible/near-infrared spectra of (a) RGO, (b) SRGO and the plot of $(\alpha h\nu)^2$ as a function of $h\nu$ for (c) RGO and (d) SRGO (see ESI, Fig. S1† for complete absorption spectra).

Nitrogen gas adsorption

Fig. 4a shows the nitrogen adsorption/desorption isotherm at 77 K for GO, RGO and SRGO. The adsorption isotherm of GO is featureless and shows a small volume of adsorbed nitrogen gas at low relative pressure (Fig. 4a, GO and inset).[34] This translates in a low specific surface areas of 25 and 15 $m^2\ g^{-1}$ according to BET and DFT Monte Carlo approaches, respectively (Table 1), which is in agreement with that reported in the literature.[35] Both unmodified and modified RGO present mixed type I and type II isotherms for low and high relative pressure (P/P_0),[9,36,37] respectively. At low P/P_0 (0–0.5), the low adsorbed volume for RGO and SRGO is characteristic of mesoporous-like material, which is confirmed by the plateau and a H3 hysteresis loop.[38,39] It can be seen that, after modification of RGO, a drop of the adsorbed volume is observed for SRGO a low relative pressure. The effect of organic molecules grafting on graphene sheets can be quantified by BET surface area (Table 1), the cumulated surface area (Fig. 4b) as well as the pore size distribution (Fig. 4c).

The BET surface area of RGO is about 900 $m^2\ g^{-1}$ and the material consists of small mesopores (2–50 nm) (Fig. 4c). The high specific surface area demonstrates that the thermal reduction with loss of oxygen functional groups created porosity. Although, it is still far below to the theoretical value for completely exfoliated and isolated graphene sheets (2630 m^2

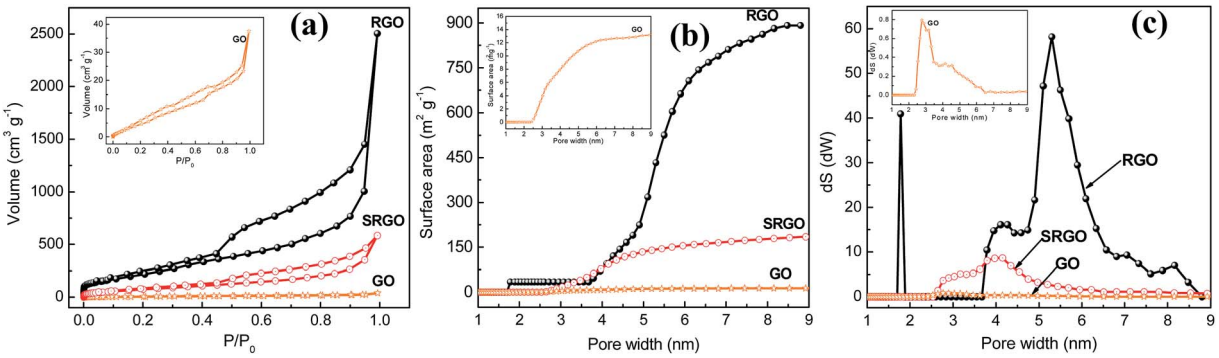

Fig. 4 (a) N_2 adsorption isotherms of graphene oxide, reduced graphene oxide before (RGO) and after reaction with *in situ*-generated 4-sulfophenyl diazonium cations (SRGO), (b) cumulated surface area *vs.* pore width of GO, RGO and SRGO, (c) pore size distribution of GO, RGO and SRGO. The insets present the data for GO at a more sensitive scale.

Table 1 Specific surface areas and electronic conductivity of graphene oxide (GO), reduced graphene oxide (RGO) and sulfophenyl-modified reduced graphene oxide (SRGO)

Sample	BET surface area ($m^2\ g^{-1}$)	DFT surface area ($m^2\ g^{-1}$)	Electronic conductivity, σ ($S\ cm^{-1}$)
GO	25	15	0.5
RGO	900	895	7.7
SRGO	300	200	2.2

g^{-1}),[4,40,41] it compares well with those published in the literature.[12,41–43] The lower value could be due to the agglomeration/precipitation and partial overlapping of reduced sheets during the thermal reduction process, which could lead to inaccessible surface.[42] Following grafting of sulfophenyl groups, the BET surface area decreased to 300 $m^2\ g^{-1}$ for SRGO (Fig. 4b and Table 1). This decrease of the BET surface area provides indirect evidence for grafting. Obviously, the attachment of organic molecules at the RGO surface causes changes in the graphene structure and creates a similar situation to that of the oxides on the surface of the graphene sheets.[44,45] The grafting block some pores of graphene sheets aggregates which make them inaccessible,[9] which creates a significant decrease of the cumulated surface area (Fig. 4b) and a noticeable difference of the pore size distribution (Fig. 4c). Interestingly, grafting of sulfophenyl groups lead to smaller pores which might be formed by the decarboxylation of groups present on RGO.[45,46]

FTIR

Fig. 5 shows the Fourier transform infrared spectroscopy (FTIR) spectra of GO, RGO and SRGO. The spectrum of GO (Fig. 5a) displays the presence of bands associated to C–O (υ_{C-O} at 1048 cm^{-1}), C–O–C (υ_{C-O-C} at 1223 cm^{-1}), C–OH (υ_{C-O-H} at 1376 cm^{-1}), C=O in carboxylic acid and carbonyl moieties that are present mostly along sheet edges but also on the basal plane of graphene sheets ($\upsilon_{C=O}$ at 1725 cm^{-1}) and a broad peak between 3000 and 3500 cm^{-1} corresponding to O–H vibration.[13,43,47] The RGO spectrum exhibits only two peaks at 1160 cm^{-1} (υ_{C-O-H}) and 1550 cm^{-1} ($\upsilon_{C=C}$), which suggests that the GO has been effectively reduced during the process. The slight shift of these two bands to higher energy indicates the restoration of the π-network.[43] The SRGO spectrum shows new bands at 1034 and 1160 cm^{-1}, which fall within the range of the symmetric and asymmetric stretching modes of $-SO_3H$ functional groups and demonstrate the presence of sulfophenyl groups on RGO.[48–50]

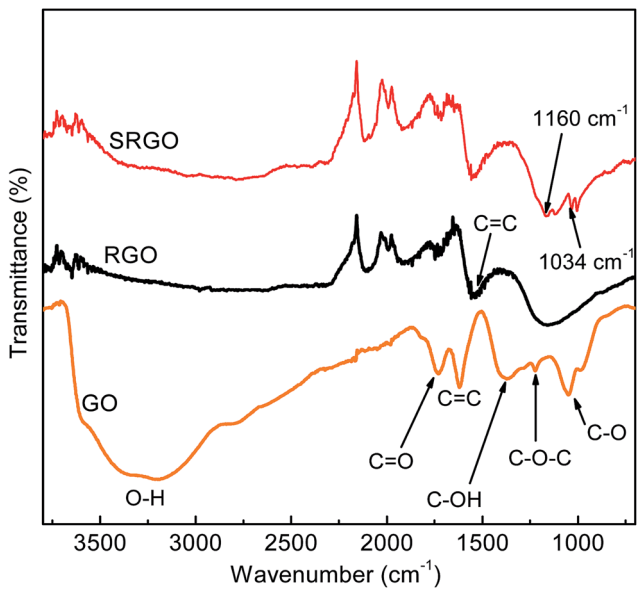

Fig. 5 FTIR curves of graphene oxide, reduced graphene oxide and sulfophenyl groups modified RGO.

Raman spectroscopy

Raman spectroscopy provides valuable information for graphene and its derivates because it is very sensitive to the electronic structure of the carbon nanostructures, therefore the degree of hybridization, the crystal disorder and the extent of chemical modification.[20,51] Fig. 6 shows the Raman spectra obtained for GO, RGO and SRGO. Each spectrum exhibits a G band corresponding to the first-order scattering of the E_{2g} mode[42] around 1600 cm^{-1} and a D band arising from the doubly resonant disorder-induced mode at ~1350 cm^{-1}.[52–56] The ratio of the intensity of these two bands (I_D/I_G) is included on the figure.

The GO sample shows a prominent D peak with a I_D/I_G of 1 indicative of significant structural disorder created due to the presence of oxygen functional groups.[57,58] Consequently, the sharp increase of the I_D/I_G ratio from ~0.09 for pristine graphite (ESI, Fig. S2†) indicates a decrease in the in-plane crystal and a partial amorphization of graphite, by conversion of sp^2 to sp^3 carbon bonds. The G peak of GO is shifted to higher energy (~19 cm^{-1}) and broadened significantly compared to that of pristine graphite (ESI, Fig. S2†).[52,56,57,59] Following thermal reduction of graphene oxide, the vibration frequency of the G band decreases to 1588 cm^{-1} (Fig. 6b), a value still slightly higher than that of pristine graphite. This phenomenon could be attributed to the influence of residual defects and isolated double bonds in RGO.[56,60] Nevertheless, the I_D/I_G ratio in this case decreases to 0.84, indicating that there were some structural changes occurring during the thermal reduction process, which did not much altered the structure of RGO but partially restored the graphitic (sp^2) network.[58] Fig. 6c shows the Raman spectrum of functionalized RGO (SRGO) by sulfophenyl groups. The increase of the I_D/I_G ratio from 0.84 to 0.95 reflects the enhancement of in disorder after grafting which is due to the transformation of sp^2 carbon to sp^3 during the covalent attachment of organic molecules on graphene sheets.[20] The slight shift of G-band (~5 cm^{-1}) to higher energy confirms the covalent grafting of organic molecules, which often isolates sp^2 C atoms.[13,53,61]

The shape and the position of 2D band of GO, RGO and SRGO spectra around 2680 cm^{-1} indicate that these graphene materials consist of few layers.[62,63] Also, it provides information on the quality of graphene oxide initially synthesized. Typically,

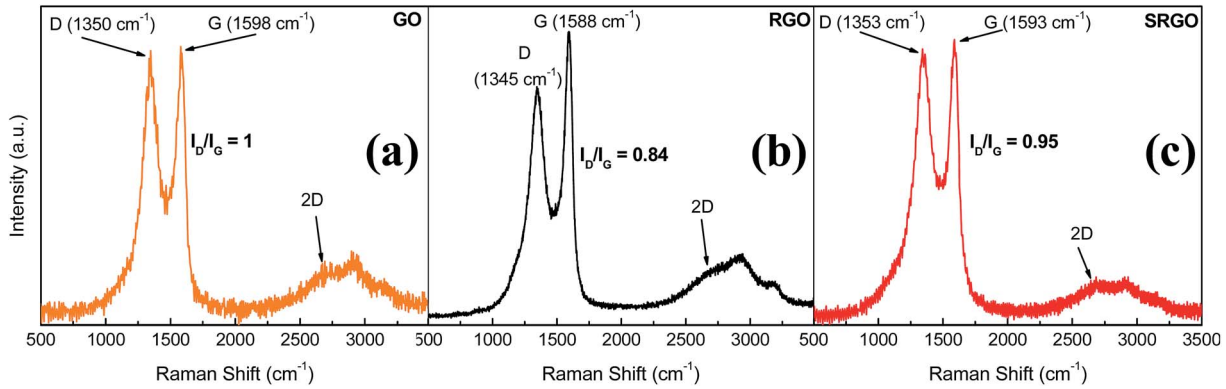

Fig. 6 Raman spectra of GO, RGO and SRGO recorded using 532 nm laser excitation.

the low intensity of 2D peak and the profile recorded in this region are the signature of graphene oxide and its derivatives.[58,64] This low intensity and broad 2D peak for GO compared with those of electrochemically exfoliated graphene (EG)[20,54] or prepared by chemical vapor deposition (CVD)[65–67] reflects the more important contribution of the steric effects of oxygen functionalities on the stacked layers as well as the partial amorphization and reduction in sp^2 domains.[43,52]

Electrical conductivity measurements

The electronic conductivities of GO, RGO and SRGO films are collected in Table 1. The low conductivity of graphene oxide (0.5 S cm^{-1}) is due to the lack of π-electronic conjugation caused by the extensive oxidation of graphite during the Hummers process.[11] The thermal reduction increases the conductivity[68,69] to 7.7 S cm^{-1}. Theoretically, the reduction of GO should firstly remove the oxygen functionalities groups, secondly rehybridize the sp^3 carbon atoms to sp^2 C and finally leave the material defects free like pristine graphene. However, no reduction method could totally restore the sp^2 structure of graphene. Then, the residual defects will affect the properties especially the electrical conductivity of RGO.[17,69–71] The higher conductivity of RGO is in good agreement with its lower I_D/I_G ratio relative to that of GO. The significant decrease of electrical conductivity of SRGO (Table 1) is related to the covalent grafting of organic molecules that converts some sp^2 C atoms to sp^3 C atoms resulting in the increase of the I_D/I_G ratio (Fig. 6c) and disruption of the π-network.

X-ray photoelectron spectroscopy (XPS)

XPS is a valuable tool for the surface chemical analysis of carbon nanostructure materials and to confirm the immobilization of the different functional groups at the graphene surface during the synthesis or its functionalization.[45,72,73] Fig. 5 shows a set of XPS spectra for GO, RGO and SRGO. The survey spectra of GO and RGO exhibit the characteristic C 1s peak at 285 eV and O 1s at 533 eV and for GO an additional small N 1s peak at 400 eV which could be related the trapping of molecular nitrogen.[62] The decrease of the O/C ratio from 0.43 to 0.11 after GO reduction to RGO demonstrates that thermal annealing eliminates most of the oxygen functionalities of graphene oxide.[18,69,75] A decrease of the intensity of N 1s peak is also noticeable. Following RGO functionalization by sulfophenyl groups, the O/C ratio increases from 0.11 to 0.17 due to the sulfonate groups ($-SO_3^-$) immobilized on graphene sheets. In addition, the SRGO survey spectrum (Fig. 3a) displays additional peaks at 230 and 167.7 eV assigned to the sulfonate groups (S 2s and S 2p, respectively).[76,77] The N 1s signal observed at 400 eV indicates the formation of azo bridges (C–N=N–C) that are commonly present in grafted modified carbon materials by using diazonium cations.[46,78–82] Their presence could be used as an indirect proof of grafting.[83] Furthermore, core level spectra were recorded for the three samples (GO, RGO and SRGO) and curve-fitted spectra are shown in Fig. 7b–h.

C 1s region. The C 1s core level spectrum of GO (Fig. 7b) shows a sp^2 component (C=C/C–C) in aromatic rings at 284.4 eV, followed by the surface oxides components (sp^3) C–OH (285.8 eV), C–O–C (286.6 eV), C=O (287.5 eV), and the carboxylate carbon (O–C=O) at 288.6 eV. Their atomic concentration (at%) are given in ESI, Table S1.†[17,42] The relative atomic concentration for different oxygenated carbon functional (C sp^3) groups is also included in Table S1† together with their counter parts from the O 1s core level spectra. The C–O species represent 50% of the total carbon atoms (Table S1†). The high oxygen content of GO is essentially related to the use of $KMnO_4$ as oxidizing agent during its preparation.[84] For RGO, its C 1s core level spectrum was fitted with five components (Fig. 7c). The contribution at 284 eV, attributed to non-oxygenated ring C, shows a significant increase of its relative area and a decrease of the FWHM (ESI, Table S1†). This suggests that the thermal treatment partially restored the π-electron network by removing most of oxygen functional groups on graphene sheets.[85] Indeed, the component observed at 286.6 eV (C–O–C) in GO spectrum (Fig. 7b), significantly decreased after thermal reduction as well as the one of C–OH at 285.8 eV (ESI, Table S1†).[64,69,85,86] This result is in good agreement with the FTIR spectra of these two materials. The C 1s XPS spectrum of RGO (Fig. 3c) also exhibits the carbonyl (C=O, 287.4 eV) and the carboxylate carbon (O–C=O, 289 eV) with peak intensities noticeably reduced in comparison to GO. However, their relative atomic concentration in terms of oxygenated carbon species (ESI, Table S1†) slightly

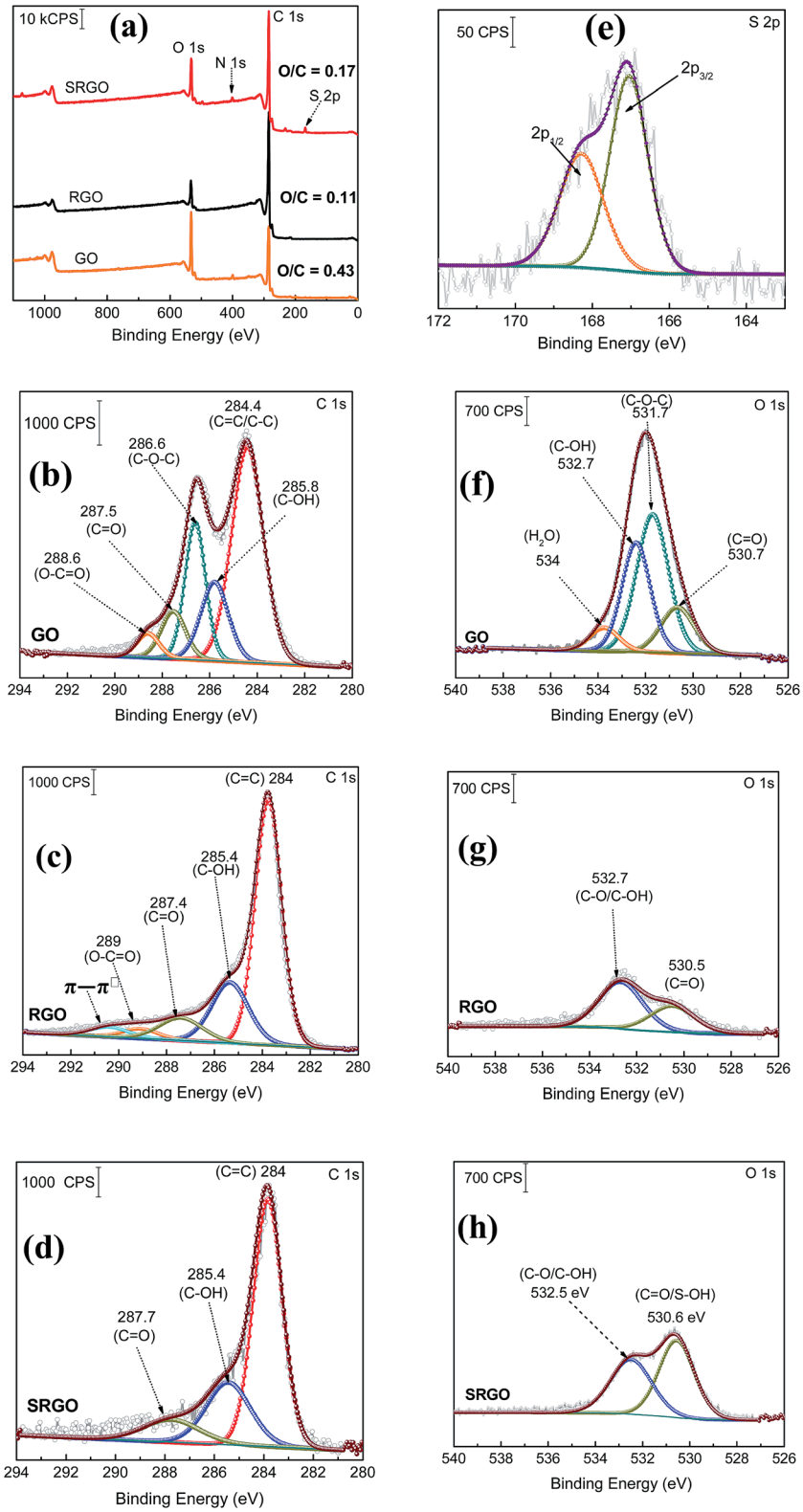

Fig. 7 (a) XPS survey spectra of graphene oxide (GO), reduced graphene oxide (RGO) and sulfophenyl-modified RGO (SRGO); XPS C 1s spectra of (b) GO, (c) RGO and (d) SRGO, (e) S 2p core level spectrum of SRGO and XPS O 1s spectra of (f) GO, (g) RGO and (h) SRGO.

increased, probably due to CO_2 blisters (especially from epoxy groups)[85] which could be trapped between graphene sheets during the annealing.[87,88] In addition, there is an additional component at 290.5 eV corresponding to shake-up satellite (π–π^*) peak or to π-electrons delocalized in the aromatic network.[89] Fig. 5d displays the C 1s core level spectrum of

modified RGO (SRGO) with sulfophenyl groups. The spectrum can be fitted with 3 major components. It can be seen that, after graphene functionalization the relative atomic concentration of C–OH (peak at 285.4 eV) increased from 66 to 78% (ESI, Table S1†), suggesting an increase of the contribution of graphene derived sp^3 carbon (the C in C–N/C–O) bonds[27,90,91] due to the reaction with sulfophenyl diazonium ions. It is also noted that the relative area of the peak around 287.7 eV decreased and the carboxylate component (O–C=O) at 289 eV in RGO spectrum (Fig. 5c) disappeared after grafting of sulfophenyl groups. The departure of the carboxylic (COOH) groups can be attributed to the decarboxylation of the carboxylic functionalities present at the RGO surface during the reduction of the diazonium cations and subsequent grafting.[45,46]

S 2p region. The core level spectrum of S 2p peak displayed in Fig. 3e can be curve-fitted with a doublet at 168.3 and 167 eV for S $2p_{1/2}$ and S $2p_{3/2}$, respectively (Fig. 7e). This confirms the presence of sulfonate groups ($-SO_3^-$) on the graphene sheets surface.[92,93]

O 1s region. The O 1s core level spectrum of graphene oxide (GO) shown in Fig. 5f can be curve-fitted with two main contributions at 531.7 and 532.7 eV corresponding to C–O–C (46%)[74,94,95] and C–O (37%), (ESI, Table S1†)[72,74,85,95,96] bonds,[85,97] respectively. A third component, located at 530.7 eV can be assigned to the ketone and quinone functionalities (C=O) in lesser amount (16%, ESI, Table S1†), which arise at the edge or bonded to the basal plane of GO as carbonyl groups.[85,98,99] The additional weaker contribution observed at 534 eV is related to water intercalation.[43,85,89,95,96,99–102] After thermal reduction of GO, two components related to C=O (530.5 eV) and C–OH (532.7 eV) became clearly visible with very low intensities (Fig. 5g)[85,89] and a noticeable decrease of the relative areas (ESI, Table S1†) because of complete loss/conversion of C–O–C groups.[103] Water molecules trapped between graphene layers,

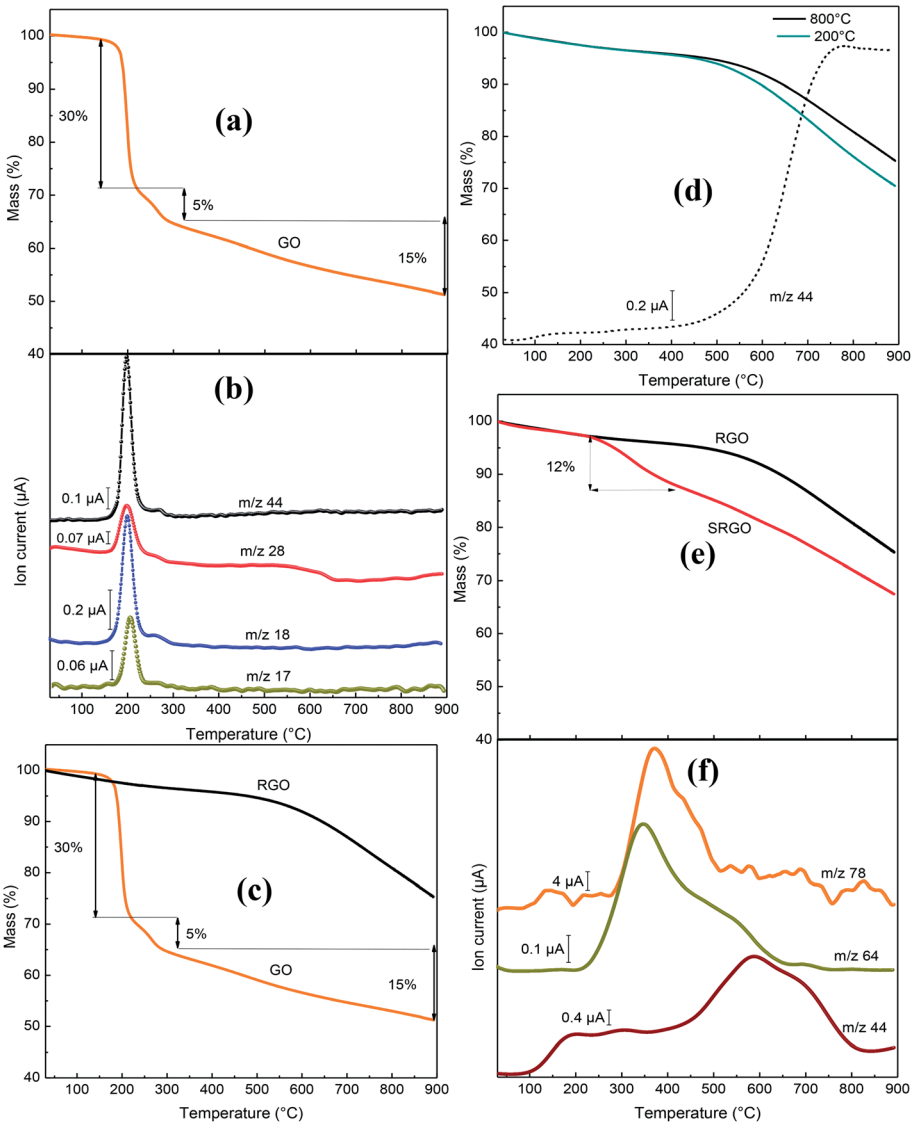

Fig. 8 (a) Mass variation for GO, (b) MS profile for GO, (c) mass variation for GO and RGO, (d) mass variation for GO following heat treatment at 200 and 800 °C, MS profile (– – –) for GO following heat treatment at 800 °C, (e) mass variation for RGO and SRGO and (f) MS profiles for SRGO.

were removed during GO thermal reduction.[85,104] Following RGO functionalization, the atomic concentration (ESI, Table S1†) and the peak intensity (Fig. 5g) of the component at 530.6 eV considerably increase. This observation is in good agreement with the introduction of the oxygenated groups attributed to S–O bonds.[73]

Thermogravimetric analysis coupled to mass spectrometry

The novelty of our work relative the vast literature existing on functionalized graphene lies in the use of TGA-MS to characterize the sulfophenyl-modified RGO. Fig. 8 shows the TGA-MS profiles of GO, RGO and SRGO under He flow. The thermogram of graphene oxide (GO) (Fig. 8a) shows a major weight loss of 35% between 170 and 300 °C, with an inflection point at 200 °C. The thermogravimetric analysis simultaneously coupled with mass spectroscopy (TGA-MS) allowed to show that the mass loss is originating from OH (m/z 17), water (m/z 18), CO (m/z 28) and CO_2 (m/z 44) release (Fig. 8b). This sudden mass loss is attributed to the removal of labile oxygen functional groups on GO sheets.[42] A weaker mass loss occurs when the temperature is increased between 300 and 900 °C and is related to the gradual removal of more stable oxygen functionalities. The TGA-MS data of GO (Fig. 8a and b) indicate that the weight loss above 300 °C can essentially be assigned to CO (m/z 28) release. The significant mass loss (~50 wt%) observed in the TGA analysis reflects the extent of the defects in the GO, which make the material thermally unstable. In contrast, RGO (obtained by thermal reduction of GO at 800 °C) show only a 5 wt% mass loss up to 500 °C, which suggests that a significant amount of labile oxygen groups were removed during heat treatment (Fig. 8c). The weight loss (20%) observed between 500 and 900 °C (Fig. 8c and d) is mostly associated to the departure of the carbonyl groups (CO_2, m/z 44) (Fig. 8d), that have not been removed during the pre-heat treatment of the GO as shown on the mass spectrum in Fig. 8c. The elimination of oxygen functionalities from GO during the pre-thermal annealing enhances the van der Waals forces attraction between graphene layers, which makes RGO thermally more stable.[17] The TGA curves of Fig. 8d show no significant difference for GO treated at 200 and 800 °C.

However, after sulfophenyl functionalization of RGO, SRGO displays a different profile compared to RGO (Fig. 8e). The onset of weight loss (~12 wt%) observed at about 350 °C is attributed to the thermal removal of organic functional groups and the weight loss is greater than that caused by the departure of only labile oxygen functionalities in this range of temperature. Two relevant fragments $m/z = 64$ (SO_2) and $m/z = 78$ (C_6H_{12}) are detected between 250 and 550 °C and correlate with the mass loss (Fig. 8e and f). The maximum of the SO_2 and C_6H_{12} peaks is around 350–400 °C, confirming the chemical bonding between graphene sheets and aryl groups.[81] The signal with m/z 44, attributed to CO_2, showed a different profile compared to unmodified RGO, with a maximum at 600 °C. The grafting of sulfophenyl groups on RGO surface is confirmed by elemental analysis (ESI, Table S2†). Their mass loading was calculated to be 12 wt% from the data in Table S2,† by considering the presence of a sulfur atom per grafted group.

4 Conclusion

Reduced graphene oxide (RGO) was synthesized *via* thermal reduction of GO under argon/hydrogen between 200 and 800 °C. Thermogravimetric analysis coupled with mass spectra analysis was firstly used to examine oxygen functionalities of GO and secondly to confirm the presence of sulfophenyl groups on the surface of chemically modified RGO. The immobilization of organic molecules on the graphene sheets was demonstrated by TEM, FTIR, XPS and nitrogen gas adsorption. Electronic conductivity measurements and Raman spectroscopy confirmed the covalent bonds between the graphene sheets and the organic molecules. The optical band gap of RGO was found to decrease following grafting of sulfophenyl groups. Finally, sulfophenyl and other aryl modified-graphene have a wide variety of potential applications. Similarly to modified carbons, SRGO and more general aryl-modified graphene could be employed in proton exchange membrane fuel cells, electrochemical capacitors, batteries, inks for printing, sensors as well as automotive and biomedical coatings.[105,106]

Conflict of interest

The authors declare no competing financial interest.

Acknowledgements

This work was financially supported by the Natural Sciences and Engineering Research Council of Canada (NSERC) by a Discovery Grant to DB. The research infrastructure of Nano-QAM was used during this work.

References

1 Z.-S. Wu, K. Parvez, X. Feng and K. Müllen, *Nat. Commun.*, 2013, **4**, 2487–3487.
2 J. H. Seol, I. Jo, A. L. Moore, L. Lindsay, Z. H. Aitken, M. T. Pettes, X. Li, Z. Yao, R. Huang, D. Broido, N. Mingo, R. S. Ruoff and L. Shi, *Science*, 2010, **328**, 213–236.
3 S. Stankovich, D. A. Dikin, G. H. B. Dommett, K. M. Kohlhaas, E. J. Zimney, E. A. Stach, R. D. Piner, S. T. Nguyen and R. S. Ruoff, *Nature*, 2006, **442**, 282–286.
4 K. S. Novoselov, A. K. Geim, S. V. Morozov, D. Jiang, Y. Zhang, S. V. Dubonos, I. V. Grigorieva and A. Firsov, *Science*, 2004, **306**, 666–669.
5 X. Zhou, Y. Li, G. Ma, Q. Ma and Z. Lei, *J. Alloys Compd.*, 2016, **685**, 216–221.
6 Q. Li, Y. Chen, J. He, F. Fu, J. Lin and W. Zhang, *J. Alloys Compd.*, 2016, **685**, 294–299.
7 D. Wei, L. Grande, V. Chundi, R. White, C. Bower, P. Andrew and T. Ryhänen, *Chem. Commun.*, 2012, **48**, 1239–1241.
8 R. Raccichini, A. Varzi, S. Passerini and B. Scrosati, *Nat. Mater.*, 2015, **14**, 271–279.
9 G. Pognon, T. Brousse and D. Bélanger, *Carbon*, 2011, **49**, 1340–1348.

10 A. Ambrosi, C. K. Chua, B. Khezri, Z. Sofer, R. D. Webster and M. Pumera, *Proc. Natl. Acad. Sci. U. S. A.*, 2012, **109**, 12899–12904.
11 W. S. Hummers and R. E. Offeman, *J. Am. Chem. Soc.*, 1958, **80**, 1339.
12 S. Park, J. An, J. R. Potts, A. Velamakanni, S. Murali and R. S. Ruoff, *Carbon*, 2011, **49**, 3019–3023.
13 J. R. Lomeda, C. D. Doyle, D. V. Kosynkin, W.-F. Hwang and J. M. Tour, *J. Am. Chem. Soc.*, 2008, **130**, 16201–16206.
14 T. Kuila, A. K. Mishra, P. Khanra, N. H. Kim and J. H. Lee, *Nanoscale*, 2013, **5**, 52–71.
15 H. J. Shin, K. K. Kim, A. Benayad, S. M. Yoon, H. K. Park, I. S. Jung, M. H. Jin, H. K. Jeong, J. M. Kim, J. Y. Choi and Y. H. Lee, *Adv. Funct. Mater.*, 2009, **19**, 1987–1992.
16 S. Pei, J. Zhao, J. Du, W. Ren and H. M. Cheng, *Carbon*, 2010, **48**, 4466–4474.
17 A. K. Das, M. Srivastav, R. K. Layek, M. E. Uddin, D. Jung, N. H. Kim and J. H. Lee, *J. Mater. Chem. A*, 2014, **2**, 1332–1340.
18 R. S. Park and S. Ruoff, *Nat. Nanotechnol.*, 2009, **4**, 217–224.
19 J. Park, S. B. Jo, Y. J. Yu, Y. Kim, J. W. Yang, W. H. Lee, H. H. Kim, B. H. Hong, P. Kim, K. Cho and K. S. Kim, *Adv. Mater.*, 2012, **24**, 407–411.
20 B. D. Ossonon and D. Bélanger, *Carbon*, 2017, **111**, 83–93.
21 S. Umrao, S. Abraham, F. Theil, S. Pandey, V. Ciobota, P. K. Shukla, C. J. Rupp, S. Chakraborty, R. Ahuja, J. Popp, B. Dietzek and A. Srivastava, *RSC Adv.*, 2014, **4**, 59890–59901.
22 L. Song, L. Ci, H. Lu, P. B. Sorokin, C. Jin, J. Ni, A. G. Kvashnin, D. G. Kvashnin, J. Lou, B. I. Yakobson and P. M. Ajayan, *Nano Lett.*, 2010, **10**, 3209–3215.
23 M. Saranya, R. Ramachandran, P. Kollu, S. K. Jeong and A. N. Grace, *RSC Adv.*, 2015, **5**, 15831–15840.
24 Y. N. Singhbabu, K. K. Sahu, D. Dadhich, A. K. Pramanick, T. Mishra and R. K. Sahu, *J. Mater. Chem. C*, 2013, **1**, 958–966.
25 X. Li, H. Zhu, J. Wei, K. Wang, E. Xu, Z. Li and D. Wu, *Appl. Phys. A: Mater. Sci. Process.*, 2009, **97**, 341–344.
26 J. Landers, G. Y. Gor and A. V. Neimark, *Colloids Surf., A*, 2013, **437**, 3–32.
27 D. S. Yu, T. Kuila, N. H. Kim, P. Khanra and J. H. Lee, *Carbon*, 2013, **54**, 310–322.
28 G. Wang, B. Wang, J. Park, Y. Wang, B. Sun and J. Yao, *Carbon*, 2009, **47**, 3242–3246.
29 Y. Zhu, M. D. Stoller, W. Cai, A. Velamakanni, R. D. Piner, D. Chen and R. S. Ruoff, *ACS Nano*, 2010, **4**, 1227–1233.
30 Y. Wang, X. Tong, X. Guo, Y. Wang, G. Jin and X. Guo, *Nanotechnology*, 2013, **24**, 1–5.
31 S. Umrao, S. Abraham, F. Theil, S. Pandey, V. Ciobota, P. K. Shukla, C. J. Rupp, S. Chakraborty, R. Ahuja, J. Popp, B. Dietzek and A. Srivastava, *RSC Adv.*, 2014, **4**, 59890–59901.
32 A. Mathkar, D. Tozier, P. Cox, P. Ong, C. Galande, K. Balakrishnan, A. Leela Mohana Reddy and P. M. Ajayan, *J. Phys. Chem. Lett.*, 2012, **3**, 986–991.
33 J. M. Englert, C. Dotzer, G. Yang, M. Schmid, C. Papp, J. M. Gottfried, H.-P. Steinrück, E. Spiecker, F. Hauke and A. Hirsch, *Nat. Chem.*, 2011, **3**, 279–286.
34 K. T. Shruthi, M. S. Kumar, A. Pratap and N. Chandrasekaran, *RSC Adv.*, 2015, **5**, 93423–93432.
35 Y. Gao, D. Ma, C. Wang, J. Guan and X. Bao, *Chem. Commun.*, 2011, **47**, 2432–2434.
36 S. Brunauer, L. S. Deming, W. E. Deming and E. Teller, *J. Am. Chem. Soc.*, 1940, **62**, 1723–1732.
37 A. Gambou-Bosca and D. Belanger, *J. Electrochem. Soc.*, 2015, **162**, A5115–A5123.
38 K. S. W. Sing and R. T. Williams, *Adsorpt. Sci. Technol.*, 2004, **22**, 773–782.
39 T. Ohkubo, J. Miyawaki, K. Kaneko, R. Ryoo and N. A. Seaton, *J. Phys. Chem. B*, 2002, **106**, 6523–6528.
40 R. F. Bruinsma, P. G. De Gennes, J. B. Freund and D. Levine, *Nature*, 2004, **427**, 523–527.
41 M. D. Stoller, S. Park, Y. Zhu, J. An and R. S. Ruoff, *Nano Lett.*, 2008, **8**, 3498–3502.
42 S. Stankovich, D. A. Dikin, R. D. Piner, K. A. Kohlhaas, A. Kleinhammes, Y. Jia, Y. Wu, S. T. Nguyen and R. S. Ruoff, *Carbon*, 2007, **45**, 1558–1565.
43 D. R. Dreyer, S. Park, C. W. Bielawski and R. S. Ruoff, *Chem. Soc. Rev.*, 2010, **39**, 228–240.
44 C. Moreno-Castilla, M. A. Ferro-Garcia, J. P. Joly, I. Bautista-Toledo, F. Carrasco-Marín and J. Rivera-Utrilla, *Langmuir*, 1995, **11**, 4386–4392.
45 M. Toupin and D. Bélanger, *Langmuir*, 2008, **24**, 1910–1917.
46 A. Le Comte, D. Chhin, A. Gagnon, R. Retoux, T. Brousse and D. Bélanger, *J. Mater. Chem. A*, 2015, **3**, 6146–6156.
47 H. Li, Y. Wang, Y. Shi, J. Li, L. H. Yanga and H. Ying, *RSC Adv.*, 2013, **35**, 14839–15492.
48 D. D. Jiang, Q. Yao, M. A. McKinney and C. A. Wilkie, *Polym. Degrad. Stab.*, 1999, **63**, 423–434.
49 J. Lu, Y. Li, S. Li and S. P. Jiang, *Sci. Rep.*, 2016, **6**, 21530–21542.
50 D. H. Johnston and D. F. Shriver, *Inorg. Chem.*, 1993, **32**, 1045–1047.
51 Z. Xia, F. Leonardi, M. Gobbi, Y. Liu, V. Bellani, A. Liscio, A. Kovtun, R. Li, X. Feng, E. Orgiu, P. Samorì, E. Treossi and V. Palermo, *ACS Nano*, 2016, **10**, 7125–7134.
52 A. C. Ferrari and J. Robertson, *Phys. Rev. B: Condens. Matter Mater. Phys.*, 2000, **61**, 14095–14107.
53 A. C. Ferrari and D. M. Basko, *Nat. Nanotechnol.*, 2013, **8**, 235–246.
54 A. C. Ferrari, J. C. Meyer, V. Scardaci, C. Casiraghi, M. Lazzeri, F. Mauri, S. Piscanec, D. Jiang, K. S. Novoselov, S. Roth and A. K. Geim, *Phys. Rev. Lett.*, 2006, **97**, 187401–187405.
55 W. Gao, M. Majumder, L. B. Alemany, T. N. Narayanan, M. A. Ibarra, B. K. Pradhan and P. M. Ajayan, *ACS Appl. Mater. Interfaces*, 2011, **3**, 1821–1826.
56 M. Fang, K. Wang, H. Lu, Y. Yang and S. Nutt, *J. Mater. Chem.*, 2009, **19**, 7098–7105.
57 M. A. Pimenta, G. Dresselhaus, M. S. Dresselhaus, L. G. Cançado, A. Jorio and R. Saito, *Phys. Chem. Chem. Phys.*, 2007, **9**, 1276–1291.
58 W. Chen and L. Yan, *Nanoscale*, 2010, **2**, 559–563.
59 Y. Wang, D. C. Alsmeyer and R. L. Mccreery, *Carbon*, 1990, **2**, 557–563.

60 K. N. Kudin, B. Ozbas, H. C. Schniepp, R. K. Prud'homme, I. A. Aksay and R. Car, *Nano Lett.*, 2008, **8**, 36–41.
61 G. Wei, M. Yan, R. Dong, D. Wang, X. Zhou, J. Chen and J. Hao, *Chem.–Eur. J.*, 2012, **18**, 14708–14716.
62 H. Lim, J. S. Lee, H. J. Shin, H. S. Shin and H. C. Choi, *Langmuir*, 2010, **26**, 12278–12284.
63 M. S. Dresselhaus, A. Jorio, M. Hofmann, G. Dresselhaus and R. Saito, *Nano Lett.*, 2010, **10**, 751–758.
64 A. Ganguly, S. Sharma, P. Papakonstantinou and J. Hamilton, *J. Phys. Chem.*, 2011, **115**, 17009–17019.
65 A. Guermoune, T. Chari, F. Popescu, S. S. Sabri, J. Guillemette, H. S. Skulason, T. Szkopek and M. Siaj, *Carbon*, 2011, **49**, 4204–4210.
66 Z. Jin, T. P. McNicholas, C. J. Shih, Q. H. Wang, G. L. C. Paulus, A. J. Hilmer, S. Shimizu and M. S. Strano, *Chem. Mater.*, 2011, **23**, 3362–3370.
67 Y. I. Zhang, L. Zhang and C. Zhou, *Acc. Chem. Res.*, 2013, **46**, 2329–2339.
68 K. Parvez, S. Yang, X. Feng and K. Müllen, *Synth. Met.*, 2015, **210**, 123–132.
69 S. Pei and H. M. Cheng, *Carbon*, 2012, **50**, 3210–3228.
70 C. Singh, A. K. Mishra and A. Paul, *J. Mater. Chem. A*, 2015, **3**, 18557–18563.
71 J. Wang, T. Zhou, H. Deng, F. Chen, K. Wang, Q. Zhang and Q. Fu, *Colloids Surf., B*, 2013, **101**, 171–176.
72 J. Guan, X. Chen, T. Wei, F. Liu, S. Wang, Q. Yang, Y. Lu and S. Yang, *J. Mater. Chem. A*, 2015, **3**, 4139–4146.
73 G. Gao, D. Liu, S. Tang, C. Huang, M. He, Y. Guo, X. Sun and B. Gao, *Sci. Rep.*, 2016, **6**, 1–8.
74 X. Fan, W. Peng, Y. Li, X. Li, S. Wang, G. Zhang and F. Zhang, *Adv. Mater.*, 2008, **20**, 4490–4493.
75 C.-Y. Su, A.-Y. Lu, Y. Xu, F.-R. Chen, A. N. Khlobystov and L.-J. Li, *ACS Nano*, 2011, **5**, 2332–2339.
76 S. Baranton and D. Bélanger, *J. Phys. Chem. B*, 2005, **109**, 24406–24410.
77 E. Lebègue, T. Brousse, J. Gaubicher and C. Cougnon, *Electrochim. Acta*, 2013, **88**, 680–687.
78 F. Hauquier, N. Debou, S. Palacin and B. Jousselme, *J. Electroanal. Chem.*, 2012, **677–680**, 127–132.
79 J. Lyskawa, A. Grondein and D. Bélanger, *Carbon*, 2010, **48**, 1271–1278.
80 D. B. Ossonon, M. Weissmann and D. Bélanger, *Electrochim. Acta*, 2014, **122**, 210–217.
81 M. Toupin and D. Bélangeer, *J. Phys. Chem. C*, 2007, **111**, 5394–5401.
82 L. Madec, K. A. Seid, J.-C. Badot, B. Humbert, P. Moreau, O. Dubrunfaut, B. Lestriez, D. Guyomard and J. Gaubicher, *Phys. Chem. Chem. Phys.*, 2014, **16**, 22745–22753.
83 C. Saby, B. Ortiz, G. Y. Champagne and D. Bélanger, *Langmuir*, 1997, **7463**, 6805–6813.
84 T. S. Sreeprasad, S. M. Maliyekkal, K. P. Lisha and T. Pradeep, *J. Hazard. Mater.*, 2011, **186**, 921–931.
85 C. Mattevi, G. Eda, S. Agnoli, S. Miller, K. A. Mkhoyan, O. Celik, D. Mastrogiovanni, C. Cranozzi, E. Carfunkel and M. Chhowalla, *Adv. Funct. Mater.*, 2009, **19**, 2577–2583.
86 S. Park, K.-S. Lee, G. Bozoklu, W. Cai, S. T. Nguyen and R. S. Ruoff, *ACS Nano*, 2008, **2**, 572–578.
87 K. Hu, X. Xie, T. Szkopek and M. Cerruti, *Chem. Mater.*, 2016, **28**, 1756–1768.
88 S. Eigler, C. Dotzer, A. Hirsch, M. Enzelberger and P. Müller, *Chem. Mater.*, 2012, **24**, 1276–1282.
89 C. Hontoria-Lucas, A. J. López-Peinado, J. de D. López-González, M. L. Rojas-Cervantes and R. M. Martín-Aranda, *Carbon*, 1995, **33**, 1585–1592.
90 A. Sinitskii, A. Dimiev, D. A. Corley, A. A. Fursina, D. V. Kosynkin and J. M. Tour, *ACS Nano*, 2010, **4**, 1949–1954.
91 A. Mesnage, X. Lefe, P. Je, G. Deniau and S. Palacin, *Langmuir*, 2012, **28**, 11767–11778.
92 J. Marwan, T. Addou and D. Bélanger, *Chem. Mater.*, 2005, **17**, 2395–2403.
93 A. L. Gui, G. Liu, M. Chockalingam, G. Le Saux, J. B. Harper and J. J. Gooding, *Electroanalysis*, 2010, **22**, 1283–1289.
94 A. Y. Romanchuk, A. S. Slesarev, S. N. Kalmykov, D. V. Kosynkin and J. M. Tour, *Phys. Chem. Chem. Phys.*, 2013, **15**, 2321–2327.
95 H. Dai, Z. Xu and X. Yang, *J. Phys. Chem. C*, 2016, **120**, 22585–22596.
96 V. Shubina, L. Gaillet, S. Ababou-Girard, V. Gaudefroy, T. Chaussadent, F. Farças, T. Meylheuc, C. Dagbert and J. Creus, *Appl. Surf. Sci.*, 2015, **351**, 1174–1183.
97 A. Ganguly, S. Sharma, P. Papakonstantinou and J. Hamilton, *J. Phys. Chem. C*, 2011, **115**, 17009–17019.
98 Y. Ishii, D. Yang, A. Velamakanni, S. J. An and M. Stoller, *Science*, 2008, **321**, 1815–1818.
99 T. Szabo, O. Berkesi, P. Forgo, K. Josepovits, Y. Sanakis, D. Petridis and I. Dékany, *Chem. Mater.*, 2006, **18**, 2740–2749.
100 G. Gunasekaran and L. R. Chauhan, *Electrochim. Acta*, 2004, **49**, 4387–4395.
101 Y. Xiong, Y. Xie, Z. Li and C. Wu, *Chem.–Eur. J.*, 2003, **9**, 1645–1651.
102 A. Buchsteiner, A. Lerf and J. Pieper, *J. Phys. Chem. B*, 2006, **110**, 22328–22338.
103 L. B. Casabianca, M. A. Shaibat, W. W. Cai, S. Park, R. Piner, R. S. Ruoff and Y. Ishii, *J. Am. Chem. Soc.*, 2010, **132**, 5672–5676.
104 C. Zhao, H. Gao, C. Chen and H. Wu, *J. Mater. Chem. A*, 2015, **3**, 18360–18364.
105 B. Desalegn, T. Brousse and D. Bélanger, *Carbon*, 2015, **92**, 362–381.
106 D. Bélanger and J. Pinson, *Chem. Soc. Rev.*, 2011, **40**, 3995–4048.

